Sains Malaysiana 46(10)(2017): 1935–1942
http://dx.doi.org/10.17576/jsm-2017-4610-32

Synthesis of γ-Fe_2O_3, Fe_3O_4 and Copper Doped Fe_3O_4 Nanoparticles by Sonochemical Method

(Sintesis γ-Fe_2O_3, Fe_3O_4 dan Tembaga Terdop dengan Nanopartikel Fe_3O_4 melalui Kaedah Sonokimia)

KANNUSAMY MOHANRAJ* & GANESAN SIVAKUMAR

ABSTRACT

Nanoparticles of undoped and copper doped with Fe_3O_4 of three concentrations (0.5, 1.0 and 1.5) are synthesized by sonochemical method. Structural, optical and morphological properties of these compounds were studied. Fe^{2+}/Fe^{3+} ratio is found to be 2.36. Crystalline structure, lattice parameters, surface morphologies, direct and indirect band gap energies of the synthesized compounds were estimated and the results are discussed in detail. The XDR analysis indicates the Cu doped Fe_3O_4 nanoparticles have higher crystallinity than undoped samples. Average crystallite size is found to increase as Cu concentration increased. The FTIR results are proven by the presence of mixed magnetite-hematite nanostructures and it is complement to the XRD results. The presence of spherical, polygonal and agglomeration forms of the particles are visually seen in the SEM images. Direct and indirect band gap energy is found to be decreased as the copper concentration was increased.

Keywords: Copper; Fe^{2+}/Fe^{3+} ratio; magnetite; sonochemical

ABSTRAK

Nanopartikel yang tidak terdop dan tembaga yang didop dengan tiga kepekatan Fe3O4 (0.5, 1.0 dan 1.5) disintesis oleh kaedah sonokimia. Struktur, sifat optik dan morfologi sebatian ini dikaji. Nisbah Fe^{2+}/Fe^{3+} yang diperoleh adalah 2.36. Struktur kristal, parameter kisi, morfologi permukaan, tenaga jurang jalur langsung dan tidak langsung daripada sebatian yang disintesis telah dianggarkan dan hasilnya dibincangkan secara terperinci. Analisis XDR menunjukkan bahawa Cu terdop dengan nanopartikel Fe3O4 mempunyai kristalografi yang lebih tinggi daripada sampel yang tidak terdop. Ukuran purata kristal didapati meningkat apabila kepekatan Cu meningkat. Keputusan FTIR dibuktikan oleh kehadiran struktur nano hematit magnetit yang bercampuran dan ia pelengkap kepada keputusan XRD. Kehadiran bentuk sfera, poligon dan aglomerasi zarah dapat dilihat secara visual dalam imej SEM. Tenaga jurang jalur langsung dan tidak langsung didapati menurun kerana peningkatan kepekatan tembaga.

Kata kunci: Magnetit; nisbah Fe^{2+}/Fe^{3+}; sonokimia; tembaga

INTRODUCTION

Nanocrystalline Fe_3O_4 is an excellent material for fabrication of magnetic record or storage devices due to its reduce saturation magnetization (Ms) 62.5-88 emu/g than that of bulk 92.6-95.5 emu/g. Many researchers have been synthesized Fe_3O_4 nanoparticles doped with Mn, Zn, Co, Al, Cu, Ag and Ni (Gupta et al. 2002; Hastings & Corliss 1956; Liu et al. 2006; Rao et al. 2007; Tripathy et al. 2008, 2007; Varshney et al. 2011; Wang et al. 2010). From their investigations, Ms was found to be either decreased or increased depends on nature of the metals and particle size. Also, Fe^{2+}/Fe^{3+} molar ratio (0.4-0.6) and iron concentration (39-78 mM) are major role in the formation of homogenous iron oxide nanoparticles under non oxidizing environment, otherwise, it may be oxidized as iron (III) hydroxide ($Fe(OH)_3$) (Laurent et al. 2008). Fe_3O_4 nanoparticles have been prepared by sonochemical (Dang et al. 2009); solvothermal (Hou et al. 2003), sol-gel (Hasanpour et al. 2012) co-precipitation (Kim et al. 2001; Sun et al. 2006; Tang et al. 2003), ultrasound-electrochemical (Cabrera et al. 2010), refluxing (Rahman et al. 2012), ultrasound-co-precipitation (Wu et al. 2011) and water in oil in water emulsion methods (Cong et al. 2008). Mizutani et al. 2008 have synthesized Fe_3O_4 nanoparticles under external heat in an autoclave for different Fe^{2+}/Fe^{3+} ratios 0.25 to 2.0. According to their report, the Fe^{2+}/Fe^{3+} ratio is an important factor to control the properties of Fe_3O_4 nanoparticles and to decrease the magnetization of Fe_3O_4 nanoparticles. The concentration of Fe^{2+} in the crystal structure strongly affects the magnetization.

Although the application of external heat should be controlled while preparing the Fe_3O_4 nanoparticles. Unless, the Fe_3O_4 particles are transformed into maghemite (200-400) and it is transformed into hematite (α-Fe_2O_3), when increase the temperature in the range of 400-700°C due to strong oxidation than in room temperature. Even though the presence of water molecules on the Fe_3O_4 is eliminated while heating, but it affects the particle size and magnetization (Darezereshki 2011; Rahman et al. 2012). Hence, the direct synthesis of iron oxide nanoparticles

without heat must be motivated. Tang et al. (2003) have shown a small oxidation of Fe_3O_4 at 0°C under illumination of argon laser. It can also be controlled the oxidation of Fe_3O_4 by flow of N_2 gas instead of argon gas. According to our literature review, a single report is found for direct preparation of γ-Fe_2O_3 particles without any organic substance by wet chemical method (Darezereshki et al. 2010), And there is no report found for preparation of γ-Fe_2O_3, Fe_3O_4 and Cu doped Fe_3O_4 nanoparticles by ultrasonic irradiation. Since, the method promoting Ms due to the cleaning the surface of nanoparticles and eliminating dead oxide layer, reduce particle size as well as induces the reactions of intermediates by cavitation (Cabrera et al. 2010). Hence, an attempt is made to synthesis of γ-Fe_2O_3, undoped and copper doped Fe_3O_4 nanoparticles by ultrasonic method at high concentration of Fe^{2+}.

Materials and Methods

Aqueous solution (25 mL) consist of 1.01 g of $FeCl_3$ (anhydrous, 96%) and 4.08 g of $FeSO_4.7H_2O$ (99%) and its Fe^{2+}/Fe^{3+} ratio is found to be 2.36. The mixture solution was vigorously stirred at room temperature for 1 h. The initial pH value was 2 and it was increased by adding NaOH into the solution. Subsequently, brown and black color precipitates was obtained for pH 9 and 12, respectively. Next, the precipitates were placed in ultrasonic bath (50 W, 40±3 kHz, ENERTECH) and ultrasonicated for 30 min and then it was filtered by proper filterant. Consequently, centrifuged and rinsed for three times using distilled water and ethanol. Finally, the obtained precipitates were dried at 120°C for 1 h. Similar steps were involved to synthesis Cu doped Fe_3O_4 for all three concentrations (0.5, 1.0 and 1.5) using $CuSO_4.5H_2O$ (99%) as precursors. The synthesis procedure is illustrated in Figure 1.

The structural characteristics of as-prepared and Cu doped nanoparticles were carried out by analyzing the X-ray diffraction (XRD) patterns using Cu Kα radiation in the range of 2θ = 10° - 80° in an X' Pert PRO diffractometer (PANalytical, Netherlands). FTIR spectra of the samples were recorded using Perkin Elmer (Spectrum Two), Fourier Transform Infrared Spectrometer (FTIR) in range of 4000 - 450 cm^{-1} with resolution of 4 cm^{-1}. A JEOL-Scanning Electron Microscopy (SEM) (JSM - 5610 LV) was used to record the micrograph for the samples. Optical absorption studies were carried out using a UV-visible spectroscopy (UV2202) in the wavelength range 300 - 800 nm.

Results and Discussion

XRD patterns of undoped γ-Fe_2O_3 and Fe_3O_4 particles are shown in Figure 2(a) & 2(b) indicates crystalline (Figure 2(a)) shows peaks at 2θ= 30.27°, 33.37°, 35.53°, 43.30°, 53.83°, 57.34°, 62.78° and 64.10° corresponds to (2 2 0), (3 0 3), (3 1 3), (4 0 0), (4 2 6), (5 1 3), (4 4 0) and (4 4 1) reflections, respectively, of tetragonal maghemite (JCPDS: 895894) which is formed at pH 9. In typical mechanism, the precursors yield considerable amount of Fe^{2+} and Fe^{3+} ions when they mixed with water. However, no precipitate is formed when the pH was 2. Hence, NaOH was added drop by drop into the solution to increase the pH from 2 to 9. Subsequently, brown color precipitate was formed and it was turned into brownish black at pH 12, due to the following chemical reactions (1, 2),

$$Fe^{2+} + 2Fe^{3+} + 8OH^- \longrightarrow Fe_3O_4 + 4H_2O \quad (1)$$

$$Fe_3O_4 + 2H^+ \longrightarrow \gamma\text{-}Fe_2O_3 + Fe^{2+} + H_2O \quad (2)$$

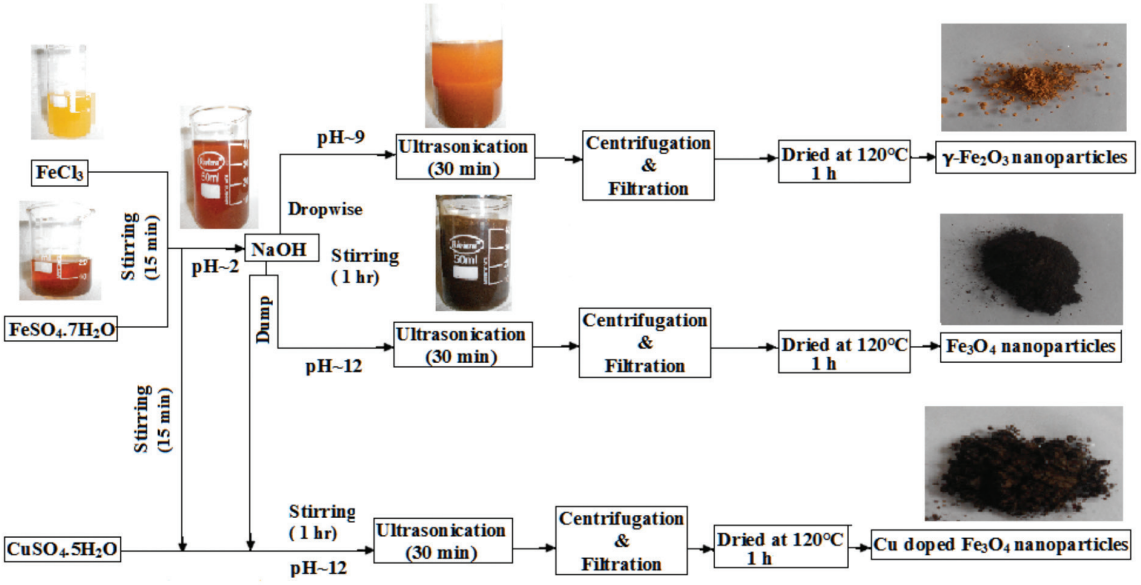

FIGURE 1. Illustration of γ-Fe_2O_3, Fe_3O_4 and Cu doped Fe_3O_4 nanoparticles

When pH of the reaction system increases $Fe(OH)_3$ and $Fe(OH)_2$ formed, which are owing to the hydrolysis of Fe^{3+} and Fe^{2+} ions, respectively. The formation of Fe_3O_4 nucleus is easier at pH<11. However, it grown easily and rapidly at pH>11 it is true in present work (Lodhia et al. 2010; Sun et al. 2006). Figure 2(b) indicates some strong crystalline peaks at 2θ = 30.37°, 35.55°, 43.20°, 53.57°, 57.05° and 62.74° corresponds to (2 2 0), (3 1 1), (4 0 0), (4 2 2), (5 1 1) and (4 4 0) reflections, respectively, of cubic structure of magnetite (JCPDS No.: 880315).

Figure 2(c)-2(e) shows the XRD patterns of copper doped Fe_3O_4 particles. It is observed that the crystalline peaks (Figure 2(c)) are shifted towards lower diffracted angles at 2θ = 30.16°, 35.48°, 43.18°, 53.58°, 57.07° and 62.69° in comparison to the undoped Fe_3O_4 with lattice parameters of a = 8.34 Å. The shift is due to replacement of Fe^{3+} ions by Cu^{2+} ions in the inverse spinal structure. Since, the ionic radius of Cu^{2+} (0.73 Å) is lower than Fe^{3+} ion (0.78 Å) (Wang et al. 2010). Hence, the crystalline structure of Fe_3O_4 is shrinked. The formation of product may be understood from (3).

$$Cu^{2+} + Fe_3O_4 \longrightarrow CuFe_2O_4 \qquad (3)$$

It can be seen from the patterns that (Figure 2(d) & 2(e)), the intensity of the cubic characteristics Fe_3O_4 peaks are increased in 1.0 M than 0.5 M whereas it is decreased in 1.5 M. It is importance to note that the diffraction pattern (Figure 2(e)) shows an additional phase due to hematite (α-Fe_2O_3) at 2θ = 24.16°, 32.18°, 33.1°, 40.85°, 49.44°, 53.96°, 57.46°, 62.38°, 63.98° and 71.75° (JCPDS No.: 89-0598). The result suggested that the increase of Cu content (1.5 M) has leads to change the crystalline structure of Fe_3O_4, hence the pattern shows heterogeneous phases. The formation of α-Fe_2O_3 may be due to the replacement of Fe^{2+} ion by Cu^{2+} ion.

The intensity of (3 1 1) reflection is strong undoped and Cu doped particles (0.5 & 1.0) indicates the product grown along (3 1 1) direction. Average crystallite size is calculated using Scherrer's formula $D = k\lambda / \beta\cos\theta$, where D is the crystalline size, k is the Scherrer's constant (k=0.9), λ is the wavelength of the X-ray, β is the full-peak width at half of the maximum (FWHM) intensity after correction for the instrument-broadening contributions and θ is the peak position. Average crystallite size is determined for the

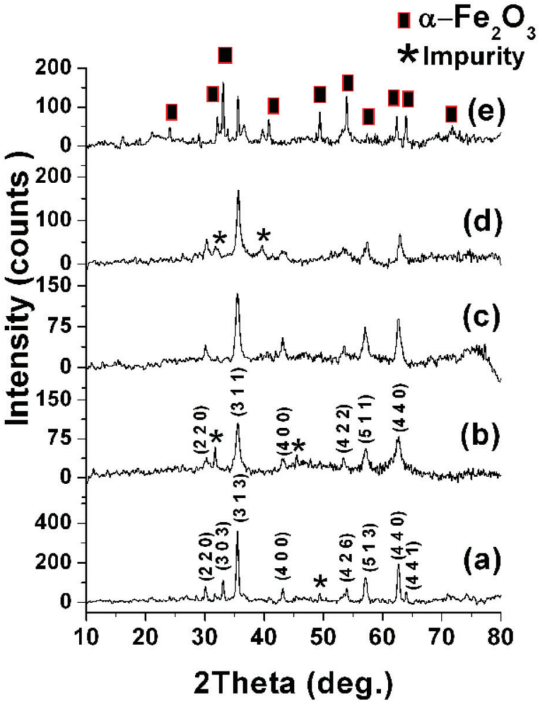

FIGURE 2. XRD patterns of synthesized (a) α-Fe_2O_3 (b) Fe_3O_4 and (c) $Cu_{0.5}Fe_3O_4$ (d) $CuFe_3O_4$ (e) $Cu_{1.5}Fe_3O_4$ nanoparticles

reflections (3 1 3) of γ-Fe_2O_3 and (3 1 1) of undoped and Cu doped Fe_3O_4 samples and its results are listed in Table 1. It is observed that the average crystallite size increases with increase in Cu concentration; it can be linked to the improvement of crystallinity and average crystallite size found to be less than 40 nm for all the samples.

Figures 3 and 4 show the FTIR spectra of undoped and Cu doped samples. In Figure 3(a), a broad band appears at 3353 cm^{-1} due to the stretching vibration of O-H (Conceicao et al. 2010). A weak broad band is shown around 1600 cm^{-1} due to bending vibration of H-O-H (Lodhia et al. 2010). A hump appears at 778 cm^{-1} and a two sharp peak are shown at 631 and 456 cm^{-1} due to Fe-O vibration. The result is in agreement well with early report on γ-Fe_2O_3 by Darezereshki et al. (2010). On comparison (Figure 3(b)), the stretching vibration of OH and H-O-H bonds are more broaden than γ-Fe_2O_3 due to in the neutral aqueous solution, the bare atoms (Fe and O)

TABLE 1. Particulars of synthesized conditions and products

Sample	Fe^{2+} / Fe^{3+} molar ratio	Concentration $CuSO_4$ (M)	1M NaOH addition	pH	Lattice parameters (Å)	Crystallite size (nm)	Colour of the precipitate
γ-Fe_2O_3	2.36	-	Drop wise	9	a= b=8.33 c=25.38	16.23	Brown
Fe_3O_4	2.36	-	Dump	12	a=b=c=8.368	19.80	Black
$Cu_{0.5}Fe_{2.5}O_4$	2.36	0.5	Dump	12	a=b=c=8.377	18.80	Black
$Cu_{1.0}Fe_{2.0}O_4$	2.36	1.0	Dump	12	a=b=c=8.346	24.36	Brownish Black
$Cu_{1.5}Fe_{1.5}O_4$	2.36	1.5	Dump	12	a=b=c=8.347	38.98	Brownish Black

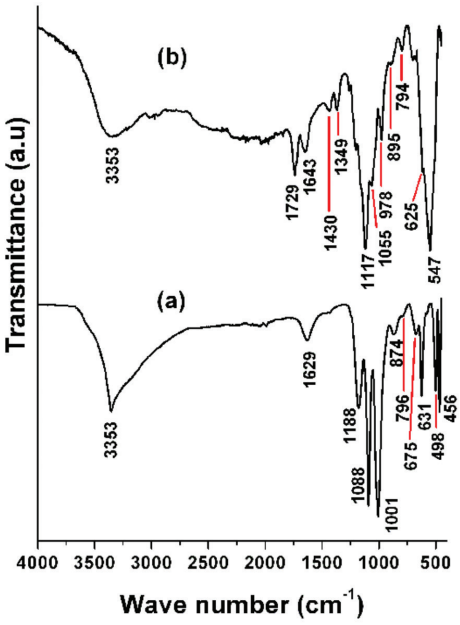

FIGURE 3. FTIR spectra of (a) α-Fe_2O_3 and (b) Fe_3O_4

would adsorb OH^- and H^+, hence ^-OH rich surface. It is also observed some peaks at 1088, 1055 and 874 cm^{-1} due to the absorption of ethanol molecules, which are present on the surface of γ-Fe_2O_3 and Fe_3O_4 nanoparticles (Dang et al. 2009; Tan et al. 2011). It may be due to washing of the products into ethanol solution and water. The dried temperature (120°C) was not sufficient to eleminate the ethanol molecules.

Figure 4(a)-4(c) shows the FTIR spectra of Cu doped Fe_3O_4 particles. It is observed from the spectrum (Figure 4(c)) the intensity of O-H and H-O-H stretching vibrations are considerably reduced in comparison to the undoped particles. A sharp and intense peak at 1113 cm^{-1} due to stretching vibration of SO_4^{2-} due to copper source and its intensity increases as Cu concentration increases. The intensity of Fe-O characteristics peaks at 895, 792, 625 and 543 cm^{-1} are increased with shift as copper concentration increases, albeit the peak at 563 cm^{-1} is decreased in 1.5 M copper concentration. It is importance to note that a peak is attributed at 615 cm^{-1} due to Cu-O vibration that confirms the presence of copper in the Fe_3O_4 product (Zarzosa et al. 2000). As similar in the XRD analysis, the 1.5 M Cu doped Fe_3O_4 shows phase changes it can be seen in the spectrum at 465 cm^{-1} due to α-Fe_2O_3 and α-FeOOH products at 3150, 1530 and 1050 cm^{-1}. In typical mechanism, the Fe^{2+} ions get oxidization due to radicals formed by decomposition of water molecules during cavitation of ultrasound. Subsequently, the Fe^{2+} ions are converted into Fe^{3+} ions and to form $Fe(OH)_3$ and FeOOH. Also excess amount of NaOH reacts with iron oxides and leading to the formation of α-Fe_2O_3 as it can be understood from the following equation (Roshan et al. 2011) (4, 5),

$$Fe^{3+} + OH^- + \tfrac{1}{2}\, O_2 \longrightarrow FeOOH \qquad (4)$$

$$2FeOOH \longrightarrow \alpha\text{-}Fe_2O_3 + H_2O \qquad (5)$$

The SEM images of the undoped and Cu doped Fe_3O_4 samples are shown in Figure 5. It can be seen from the images that the undoped particles demonstrate agglomeration form due to the magnetic interaction the particles. It is observed that smaller size grains are found to be ≈0.1 μm and 0.23 μm for large size grains. The Cu doped

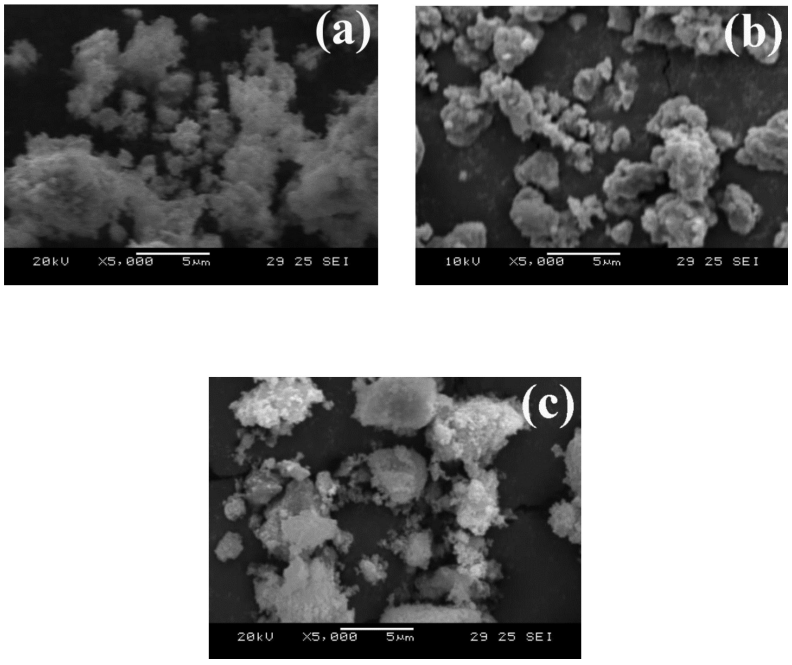

FIGURE 4. (a) $Cu_{0.5}Fe_3O_4$ (b) $CuFe_3O_4$ and (c) $Cu_{1.5}Fe_3O_4$ nanoparticles

Fe_3O_4 particles constitute almost similar agglomeration form with spherical grains as that of undoped samples. It can be seen that inhomogeneous particles were distributed over the surface. Smaller size particles are found to be 0.1 and 0.5 μm for large size particles. It is evidence from the SEM images that the Cu doped particles are increased in size in comparison to the undoped sample. This inference can be linked to the variation seen in crystallite size with increasing Cu doping from the XRD results.

The presence of NaOH plays an important role not only controls the particles size but also form iron oxide polymorphs nanoparticles. It can be interpreted with the literature (Laurent et al. 2008), that slow, constant and small drops addition of ammonia solution is influenced to obtain uniform and small size particles. This is due to the fact that small drops have a relatively small reacting constant surface and contain less reactant so that the molecules are more evenly dispersed into the solution. The space between the molecules are increased, hence, the collisions between the molecules are slower. Also, the drop by drop addition of NaOH solution leads to small size particles than that of dumping into the precursor solution. At high Cu concentration, the particles size and crystallinity is increased due to excess formation of $Fe(OH)_2$ than 0.5M in which reaction rate is relatively slow at room temperature.

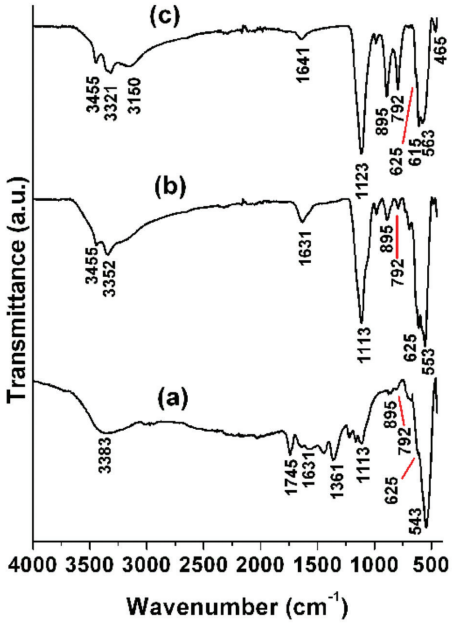

FIGURE 5. SEM micrographs of (a) α-Fe_2O_3 (b) Fe_3O_4 and (c) $CuFe_3O_4$ particles

Figure 6(a)-6(e) shows the optical absorption spectra of undoped and copper doped Fe_3O_4 particles. It can be seen from the absorption spectra that the undoped particles shows strong absorption in the range of 300-450 nm and maximum around 330 nm, due to both absorption and scattering of UV- visible radiation by the magnetic nanoparticle. The result is consistent with the early reports on Fe_3O_4 by Rahman et al. (2012) and Tang et al. (2003). In Cu doped Fe_3O_4 particles (Figure 6(c)-6(e)), the optical absorption maximum is shifted to visible region and also it is found to be decreased with increase in copper concentration, albeit 1.0 M concentration exhibit higher optical absorption than 0.5 M and 1.5 M. Trivially one can immediately correlate these spectra with the result of SEM micrograph and identify the absorption in the range of 330-450 nm due to nano size spherical grains present in the samples.

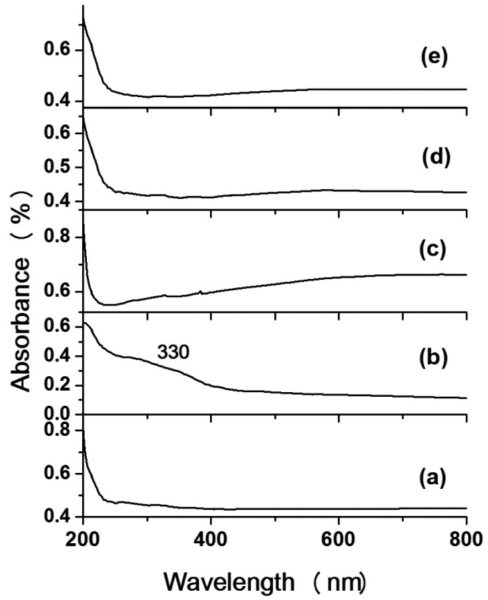

FIGURE 6. UV-Vis absorption spectra of (a) α-Fe_2O_3 (b) Fe_3O_4 and (c) $Cu_{0.5}Fe_3O_4$ (d) $CuFe_3O_4$ (e) $Cu_{1.5}Fe_3O_4$ particles

Davis and Mott have given an expression for the absorption coefficient, α (ν), as a function of photon energy (hν) for indirect and direct transition using the equation given as follows (Ghandoor et al. 2012).

$$A = -\ln(I/I_0) = \alpha(\nu)L$$

$$\alpha(\nu) = A/L$$

$$\alpha(\nu) = \alpha_0 (h\nu - E_g)^n / h\nu$$

where A is the absorption; I is intensity of transmitted light; I_0 is intensity of incident light; α (ν) is the absorption coefficient of the sample; L is the thickness of the cell; α_0 is constant related to the extent of the band tailing; E_g is optical band gap energy; and the exponent n = 1/2 for direct transition; and while n = 2 for indirect transition. The optical band gap energy for indirect and direct transition can be determined by plotting $(\alpha h\nu)^{1/2}$ and $(\alpha h\nu)^2$ as a function of photon energy (hν), respectively. The band gap energy is determined by extrapolating the straight portion of the plot to the energy axis (Figures 7-10).

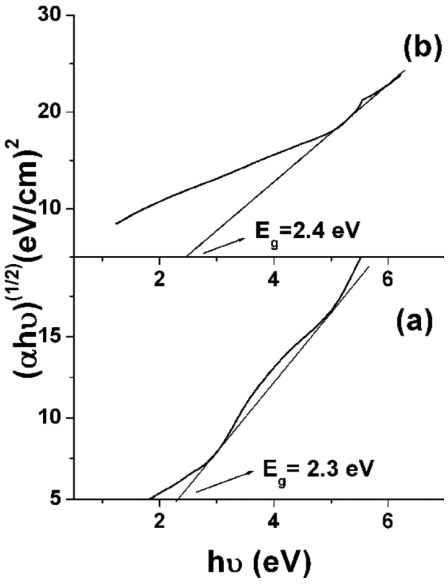

FIGURE 7. The plot of $(\alpha h\nu)^{1/2}$ Vs (hν) direct band gap of (a) α-Fe_2O_3 and (b) Fe_3O_4 particles

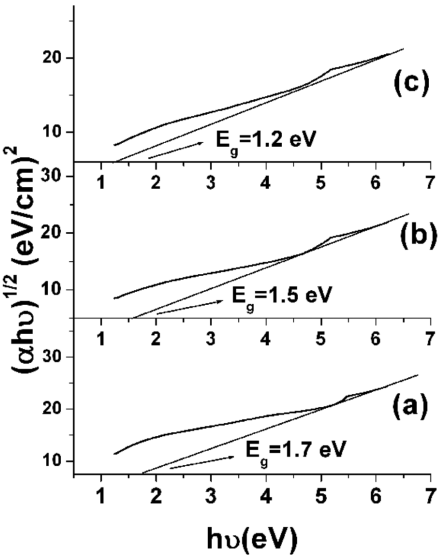

FIGURE 9. The plot of $(\alpha h\nu)^{1/2}$ Vs (hν) direct band gap of (a) $Cu_{0.5}Fe_3O_4$ (b) $CuFe_3O_4$ (c) $Cu_{1.5}Fe_3O_4$ particles

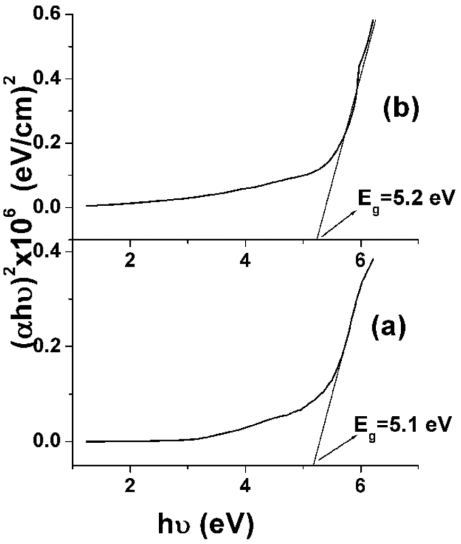

FIGURE 8. The plot of $(\alpha h\nu)^2$ Vs (hν) indirect band gap of (a) α-Fe_2O_3 and (b) Fe_3O_4 particles

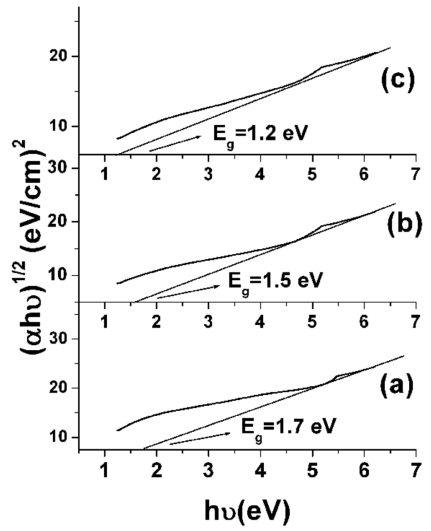

FIGURE 10. The plot of $(\alpha h\nu)^2$ Vs (hν) indirect band gap of (a) $Cu_{0.5}Fe_3O_4$ (b) $CuFe_3O_4$ and (c) $Cu_{1.5}Fe_3O_4$ particles

TABLE 2. Band gap values of the prepared nanoparticles

Sample	Direct band gap Energy (eV)	Indirect band gap Energy (eV)
γ-Fe_2O_3	2.4	5.2
Fe_3O_4	2.3	5.1
$Cu_{0.5}Fe_{2.5}O_4$	1.7	4.8
$Cu_{1.0}Fe_{2.0}O_4$	1.5	4.7
$Cu_{1.5}Fe_{1.5}O_4$	1.2	4.6

From Table 2, the band gap energy is found to be 2.4 eV for γ-Fe_2O_3 and 2.3 eV for Fe_3O_4 which is higher than bulk γ-Fe_2O_3 (2.2 eV) and Fe_3O_4 (0.1 eV) (Cornell & Schwertmann 2003). Albeit, it is found to be decreased considerably from 1.7 to 1.2 eV in the Cu doped samples. It can be correlated with the obtained crystallite size in the XRD analysis and grain size in SEM analysis. The result is evidenced that the Cu dopant plays an important role to tune the band gap energy of the Fe_3O_4 particles.

It is learnt from the early report that the mixed magnetite-hematite nanoparticles have strong adsorption of heavy metals such as lead, chromium and cadmium from the waste waters and also it have very low Ms (11 emu/g). Note that, the present work (1.5 M Cu concentration) also exhibit mixed magnetite-hematite nanostructures and low band gap energy. Therefore, the particles may have lesser Ms due to diamagnetic property of Cu. Hence, further investigation is needed to elucidate the magnetization properties of the characteristics nanoparticles; it can be used to find the sorbent efficiency. From the experimental results, the 1.5 M Cu concentration is suitable ratio to obtain mixed phase of Fe3O4 nanoparticles. It is also interesting to note that at low Cu concentration (0.5 and 1.0 M) Fe^{3+} ions are replaced by Cu^{2+} ions whereas at higher concentration (1.5 M) Fe^{2+} ions are replaced by Cu^{2+} ions, to form α–Fe_2O_3.

Conclusion

The maghemite (γ-Fe_2O_3), magnetite (Fe_3O_4) and copper doped Fe_3O_4 nanoparticles are synthesized by sonochemical method the Fe^{2+}/Fe^{3+} ratio was found 2.36. The XDR analysis indicates the Cu doped Fe_3O_4 nanoparticles have higher crystallinity than undoped samples. The higher Cu concentration (1.5 M) shows mixed magnetite-hematite nanostructures that are very useful for removal of heavy metals from the waste water. Average crystallite size is found to be increased as Cu concentration increases. The lattice parameters a, b and c are stretched or compressed. The FTIR results are proved by the presence of mixed magnetite-hematite nanostructures and it is complement to the XRD results. The presence of spherical, polygonal and agglomeration forms of the particles are visually seen in the SEM images and the observed average grain size is comparable to the crystallite size found in XRD analysis. Direct and indirect band gap energy is found to be decreased as increase the copper concentration and inversely proportional to its crystallite size.

Acknowledgements

The authors are thankful to the DST-FIST and UGC-SAP, New Delhi for providing the financial support to the Department of Physics, Manonmaniam Sundaranar University and the Prof. and Head, Department of Physics, Annamalai University for their supporting to record the SEM photographs.

References

Cabrera, L., Gutiérrez, S., Herrasti, P. & Reyman, D. 2010. Sonoelectrochemical synthesis of magnetite. *Physics Procedia* 3: 89-94.

Conceicao, T.F.D., Scharnag, l.N., Blawert, C., Dietzel, W. & Kainer, K.U. 2010. Surface modification of magnesium alloy AZ31 by hydrofluoric acid treatment and its effect on the corrosion behavior. *Thin Solid Films* 518: 5209-5218.

Cong, Y., Wang, G., Xiong, M., Huang, Y., Hong, Z., Wang, D., Li, D. & Li, L. 2008. A facile interfacial reaction route to prepare magnetic hollow spheres with tunable shell thickness. *Langmuir* 24: 6624-6629.

Cornell, R.M. & Schwertmann, U. 2003. *The Iron Oxide: Structure, Properties, Reaction, Occurrences and Uses*. 2nd ed. (Chapter 6). Federal Republic of Germany: Wiley-VCH Verlag GmbH.

Dang, F., Enomoto, N., Hojo, J. & Enpuku, K. 2009. Sonochemical synthesis of monodispersed magnetite nanoparticles by using an ethanol-water mixed solvent. *Ultrasonics Sonochemistry* 16: 649-654.

Darezereshki, E. 2011. One-step synthesis of hematite (α-Fe_2O_3) nanoparticles by direct thermal- decomposition of maghemite. *Materials Letter* 65: 642-645.

Darezereshki, E., Ranjibar, M. & Bakhitiari, F. 2010. One-step synthesis of maghemite (γ-Fe_2O_3) nanoparticles by wet chemical method. *Journals of Alloy Compounds* 502: 257-260.

Ghandoor, H.E., Zidan, H.M., Khalil, M.M.H. & Ismail, M.I.M. 2012. Synthesis and some physical properties of magnetite nanoparticles. *International Journal of Electrochemical Science* 7: 5734-5745.

Gupta, R., Sood, A.K., Metcalf, P. & Honig, J.M. 2002. Raman study of stoichiometric and Zn-doped Fe_3O_4. *Physics Review B* 65: 104430-104438.

Hasanpour, A., Niyaifar, M. & Asan, M. 2012. Synthesis and characterization of Fe_3O_4 & ZnO nanocomposites by sol-gel method. *Proceedings of the 4th International Conferences on Nanostructures (ICNS4)*, 12-14 March. pp. 205-207.

Hastings, J.M. & Corliss, L.M. 1956. Neutron diffraction study of manganese ferrite. *Physics Review* 104: 329-331.

Hou, Y., Yu, J. & Gao, S. 2003. Solvothermal reduction synthesis and characterization of superparamagnetic magnetite nanoparticles. *Journal of Material Chemistry* 13: 1983-1987.

Laurent, S., Forge, D., Port, M., Roch, A., Robic, C., Elst, L.V. & Mullerm, R.N. 2008. Magnetic iron oxide nanoparticles: Synthesis, stabilization, vectorization, physicochemical characterizations and biological applications. *Chemistry Review* 108: 2064-2110.

Liu, S.H., Tai, H.M., Pao, C.W., Chiou, J.W., Ling, D.C., Pong, W.F., Tasi, M-H., Lin, H.J., Jang, L.Y., Lee, J.F., Hsu, J.H., Wang, W.J. & Hsu, C.J. 2006. Electronic and magnetic properties of the Ag-doped Fe_3O_4 films studied by X-ray absorption spectroscopy. *Applied Physics Letter* 89: 092112.

Lodhia, J., Mandarano, G., Ferris, N.J., Eu, P. & Cowell, SF. 2010. Development and use of iron oxide nanoparticles (Part1): Synthesis of iron oxide nanoparticles for MRI. *Biomedical Imaging and Intervention Journal* 6: e12.

Roshan, A.H., Vaezi, M.R., Shokuhfur, A. & Rajabali, Z. 2011. Synthesis of iron oxide nanoparticles via sonochemical method and their characterization. *Particuology* 9: 95-99.

Sun, J., Zhou, S., Hou, P., Yang, Y., Weng, J., Li, X. & Li, M. 2006. Synthesis and characterization of biocompatible Fe_3O_4

nanoparticles. *Journal of Biomedical Materials Research Part A* 80(2): 333-341.

Tan, J., Yang, L., Kang, Q. & Cai, Q. 2011. *In situ* ATR-FTIR and UV-visible spectroscopy study of photocatalytic oxidation of ethanol over TiO_2 nanotubes. *Analytical Letters* 44: 1114-1125.

Tang, J., Myers, M., Bosnick, K.A. & Brus, L.E. 2003. Magnetic Fe_3O_4 nanocrystals: Spectroscopic observation of aqueous oxidation kinetics. *Journal of Physical Chemistry B* 107: 7501-7506.

Tripathy, D., Adeyeye, A.O., Boothroyd, C.B. & Shannigrahi, S. 2008. Microstructure and magneto transport properties of Cu doped Fe_3O_4 films. *Journal of Applied Physics* 103: 07F701-07F703.

Tripathy, D., Adeyeye, A.O., Boothroyd, C.B. & Piramanmayagam, S.N. 2007. Magnetic and transport properties of Co-doped Fe_3O_4 films. *Journal of Applied Physics* 101: 013904.

Varshney, D., Verma, K. & Yogi, A. 2011. Structural and magnetic properties of Mn and Zn doped Fe_3O_4 nanoparticles. *AIP Conference Proceedings* 1349: 253-254.

Wang, X., Hu, C.G., Xi, Y., Xia, C.H. & He, X.S. 2010. Al-doped Fe_3O_4 nanoparticles and their magnetic properties. *Journal of Superconductivity and Novel Magnetism* 23: 909-911.

Wu, S., Sun, A., Zhai, F., Wang, J., Xu, W., Zhang, Q. & Volinsky, A.A. 2011. Fe_3O_4 magnetic nanoparticles synthesis from tailings by ultrasonic chemical co-precipitation. *Materials Letters* 65: 1882-1884.

Zarzosa, G.O., Martinez, J.R., Espinos, O.D., Ruiz, F. & Aquino, J.A.M. 2000. Formation of copper based particles trapped in a silica xerogel matrix. *Superficies y vacio* 11: 61-65.

Kannusamy Mohanraj*
Department of Physics
Manonmaniam Sundaranar University
Tirunelveli-627 012, Tamilnadu
India

Ganesan Sivakumar
CISL, Department of Physics
Annamalai University
Annamalai Nagar-608 002, Tamilnadu
India

*Corresponding author; email: kmohanraj.msu@gmail.com

Received: 10 February 2014
Accepted: 1 March 2017